



Synthesis, crystal structure, electrochemistry and studies on protein binding, antioxidant and biocidal activities of Ni(II) and Co(II) hydrazone complexes

P. Sathyadevi^a, P. Krishnamoorthy^a, M. Alagesan^a, K. Thanigaimani^b, P. Thomas Muthiah^b, N. Dharmaraj^{a,*}

^a Department of Chemistry, Bharathiar University, Coimbatore 641 046, India

^b School of Chemistry, Bharathidasan University, Tiruchirappalli 620 024, India

ARTICLE INFO

Article history:

Received 5 July 2011

Accepted 16 September 2011

Available online 22 September 2011

Keywords:

Metal hydrazone complex

Crystal structure

Protein interaction

Antioxidant

Antimicrobial

ABSTRACT

Bivalent transition metal hydrazone complexes of the composition $[\text{Ni}(\text{L}_1)_2]$ (**1**), $[\text{Co}(\text{L}_1)_2]$ (**2**), $[\text{Ni}(\text{L}_2)_2]$ (**3**) and $[\text{Co}(\text{L}_2)_2]$ (**4**) have been synthesised from the reactions of $[\text{MCl}_2(\text{PPh}_3)_2]$ (where M = Ni or Co) with hydrazones derived from 2-acetyl pyridine and carboxylic acid hydrazides of benzhydrazide (**HL**₁) or thiophene-2-carboxylic acid hydrazide (**HL**₂), respectively. Structure of the ligands **HL**₁ and **HL**₂ and their corresponding complexes with Ni(II) and Co(II) ions were proposed based on the elemental analysis, infrared and ¹H NMR spectral methods. Single crystal X-ray diffraction study of complex **1** revealed a distorted octahedral geometry around the metal ion provided by two units of the ligand. To explore the potential medicinal value of the new complexes, binding interaction of all the complexes with bovine serum albumin (BSA) was studied at normal physiological conditions using fluorescence and UV–Vis spectral techniques. The number of binding sites (*n*) and binding constant (*K*_d) were calculated according to the double logarithm regression equation. The results of synchronous fluorescence spectrum showed that binding of metal hydrazones with BSA induced conformational changes in BSA. The *in vitro* antioxidant and antimicrobial potentials of the new chelates were also carried out.

© 2011 Elsevier Ltd. All rights reserved.

1. Introduction

Metal ions, especially those of bivalent type, distribute in human blood and play an essential structural role in binding with many proteins. They have a definite ability to bind proteins and affect the binding of drugs to albumin through their coordinate bonds. Investigation on the effect of metal ions on drug–albumin binding is useful to understand the transport and mechanism of the drug in the body [1,2]. Bovine serum albumin (BSA) is a protein with hydrophobic patches that could be the initial targets of their association to biomolecules [3]. Among various bio-macromolecules, serum albumins are the most abundant soluble proteins in the circulatory system of a wide variety of organisms and have many indispensable physiological functions. Serum albumins often increase the apparent solubility of hydrophobic compounds in plasma and modulate their delivery to cells. Therefore, the absorption, distribution, metabolism and excretion properties, as well as the stability and toxicity of chemical substances can be significantly affected because of their binding to serum albumins [4]. The interactions of drugs with any protein normally result in the formation of a

stable drug–protein complex that can exert important effect on the distribution, free concentration and metabolism of the drug in the blood stream. Thus the drug–albumin complex may be considered as a model for gaining fundamental insights into the drug–protein interactions. In this regard, bovine serum albumin (BSA) was studied extensively in the past years, partly because of its structural homology with human serum albumin (HSA) [5,6]. Moreover, there is evidence of conformational changes of serum albumin induced by its interaction with low molecular weight molecules that in turn affect the secondary and tertiary structure of albumins [7]. Many drugs including anti-coagulants, tranquilizers, anti-allergic drugs, anti-cancer drugs etc., are transported in the blood while bound to albumin [8]. This has stimulated much interest in the nature of binding sites and investigations of whether fatty acids, natural metabolites and drugs compete with one another for binding to the protein [9]. Therefore, studies on the binding of chemicals with protein will aid interpretation of the metabolism and transport process of them and will help to explain the relationship between the structure and the function of the protein.

Hydrazones are important class of ligands with interesting ligation properties due to the presence of several coordination sites [10] and are widely applied in the field of insecticides, medicines and analytical reagents due to their excellent bioactivity [11]. Various important properties of carbonic acid hydrazides along with

* Corresponding author. Tel.: +91 422 2428316; fax: +91 422 2422387.

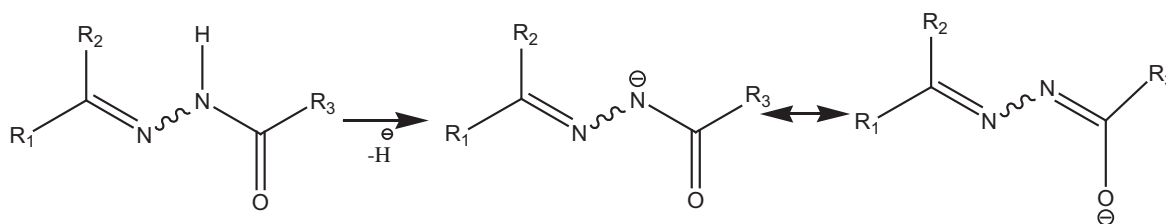
E-mail address: dharmaraj@buc.edu.in (N. Dharmaraj).

their applications in medicine and analytical chemistry have led to increased interest in their complexation characteristics with transition metal ions [12]. In this respect, the formation of metal complexes plays an important role to enhance their biological activity [13].

Studies have also shown that the azomethine nitrogen which has a lone pair of electrons in a sp^2 hybridised orbital has considerable biological importance. Hydrazone derivatives are found to possess antimicrobial, anti-tubercular, anti-convulsant and anti-inflammatory activities [14–19]. Some hydrazone analogs have been investigated as potential oral iron chelating drugs for the treatment of genetic disorders such as thalassemia and have also been suggested as possible metal chelating agents for treating neurodegenerative disorders such as Alzheimer disease [20–22].

emission spectra were recorded on Jasco FP 6600 spectrofluorometer using methanol as a solvent. Cyclic voltammetric study of the complexes was conducted in methanol using CH instrument electrochemical analyzer with tetrabutylammonium perchlorate (TBAP) as supporting electrolyte. All the solutions were purged with nitrogen prior to measurements at room temperature. A three-electrode configuration that comprised of glassy carbon as a working electrode, platinum wire as an auxiliary electrode and an Ag/AgCl electrode as a reference electrode were used.

The X-ray diffraction data of the complex **1**, were collected at 293 K with $MoK\alpha$ radiation ($\lambda = 0.71073 \text{ \AA}$) using a Bruker Smart APEX II CCD diffractometer equipped with graphite monochromator. The structure was solved by direct method and refined using full-matrix least squares (on F^2) SHELXS97 and SHELXL97 [23] and



General formula of deprotonable acyl- /aroyl- hydrazones and mesomerism of the anion obtained by deprotonation.

Detailed literature survey reveals that attempts have not been made so far to investigate the interaction of metal hydrazone chelates **1–4** with BSA. In continuation of our interest in the chemistry and biology of transition metal hydrazone chelates, we carried out a systematic work to synthesize, characterize and to investigate the interaction of Ni(II) and Co(II) hydrazone complexes with BSA. The nature of binding between the chelates and BSA were monitored through fluorescence and synchronous spectroscopy. *In vitro* antioxidant and antimicrobial activities of the free ligands as well as the metal chelates involved in this study have also been assessed and compared with that of commercial standards.

2. Experimental

2.1. Materials

$NiCl_2 \cdot 6H_2O$, $CoCl_2 \cdot 6H_2O$, triphenylphosphine (Sigma–Aldrich chemie), 2-acetyl pyridine and thiophene-2-carboxylic acid hydrazide (Alfa Aesar) were obtained commercially and used without any purification. Bovine serum albumin (BSA) was obtained from Himedia. Solvents used for the synthesis were purified by standard methods. All the other chemicals and reagents used for protein binding, antioxidant and antimicrobial studies were of high quality and commercially purchased from reputed suppliers.

2.2. Physical measurements

Microanalyses (% C, H and N) were performed on a Vario EL III CHNS analyzer. Melting points were determined with Raaga apparatus. Infrared spectra of the samples were recorded as KBr pellets on a Nicolet Avatar model in the range of $400\text{--}4000 \text{ cm}^{-1}$. 1H NMR spectra of the ligands were recorded with a Bruker AMX 500 instrument operating at 500 MHz using $CDCl_3$ as a solvent and TMS as an internal standard. Electronic spectra were recorded on Jasco V-630 spectrophotometer using methanol as a solvent. The

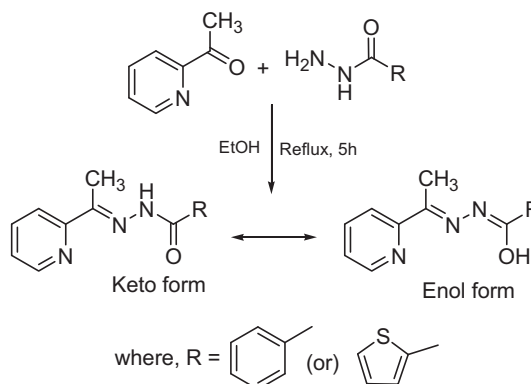
graphics were produced using PLATON97 [24]. All the non-hydrogen atoms were refined anisotropically and the hydrogen atoms were positioned geometrically and refined as riding model.

2.3. Synthesis of starting metal complexes

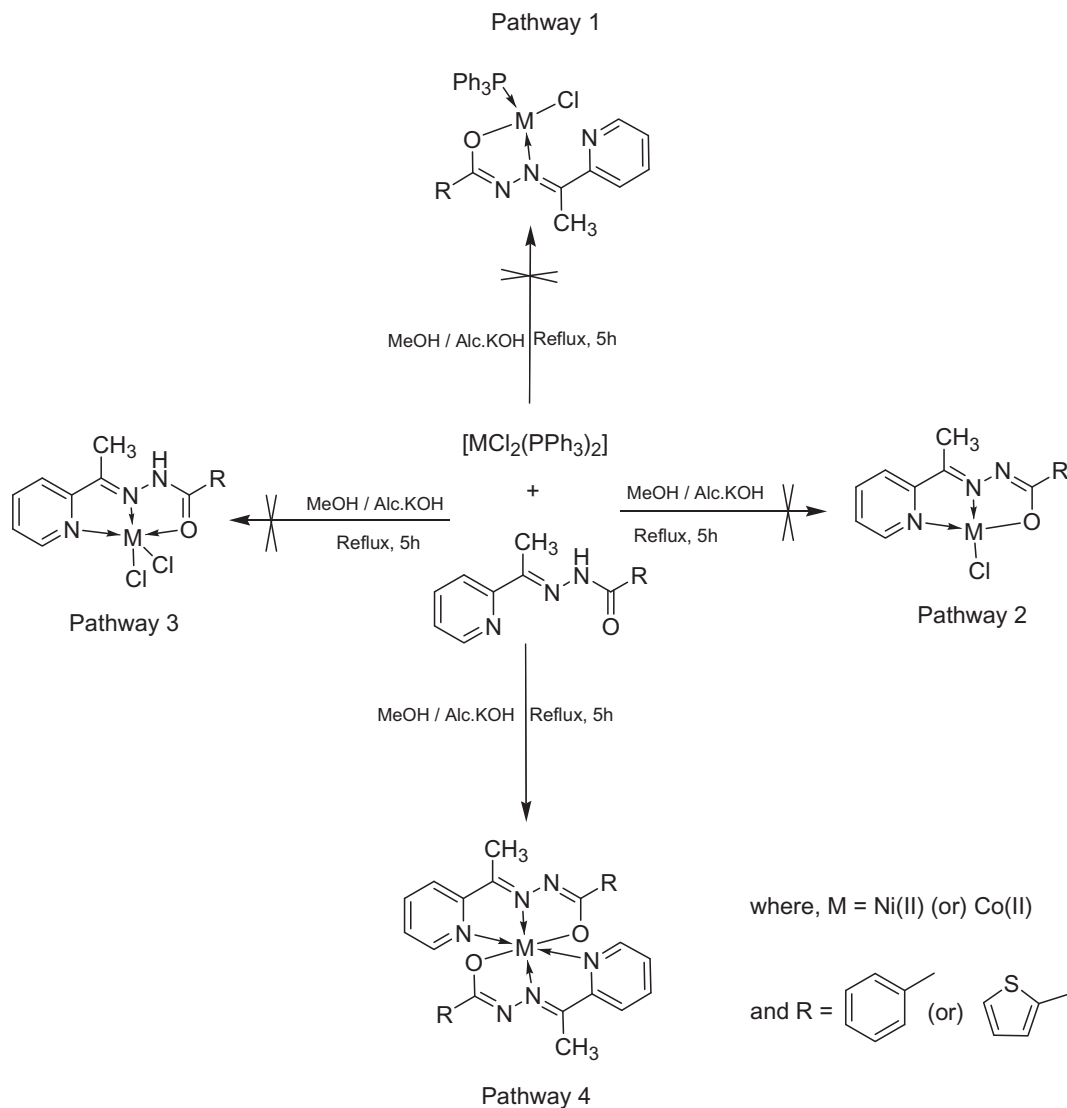
The precursor metal complexes $[NiCl_2(PPh_3)_2]$ and $[CoCl_2(PPh_3)_2]$ were prepared according to the literature methods [25,26].

2.4. Synthesis of $[N'-(1\text{-pyridin-2-yl)ethylidene}]\text{benzohydrazide}$ (**HL**₁) and $[N'-(1\text{-pyridin-2-yl)ethylidene}]\text{thiophene-2-carbohydrazide}$ (**HL**₂) ligands

The hydrazone ligands **HL**₁ and **HL**₂ were prepared by mixing equimolar (10 mmol) amounts of 2-acetylpyridine with benzhydrazide and thiophene-2-carboxylic acid hydrazide in ethanol (50 ml) as shown in Scheme 1. The reaction mixture was then re-



Scheme 1. Synthesis of hydrazone ligands.



Scheme 2. Synthesis of metal hydrazone complexes.

fluxed on a water bath for 5 h and cooled to room temperature. The hydrazones formed were filtered, washed and recrystallized from ethanol and the purity was checked by TLC.

For **HL₁**: Yield, 90%. M.p. 168 °C. *Anal. Calc.* for C₁₄H₁₃N₃O₁: C, 70.21; H, 5.43; N, 17.56. Found: C, 69.89; H, 5.18; N, 17.41%.

For **HL₂**: Yield, 88%. M.p. 166 °C. *Anal. Calc.* for C₁₂H₁₁N₃O₁S₁: C, 58.75; H, 4.52; N, 17.12; S, 13.07. Found: C, 58.46; H, 4.58; N, 17.27; S, 13.25%.

2.5. Synthesis of new hydrazone metal complexes

Complexes [Ni(L₁)₂] (**1**), [Co(L₁)₂] (**2**), [Ni(L₂)₂] (**3**) and [Co(L₂)₂] (**4**) have been synthesised from the reactions of equimolar amount of ligand **HL₁** (0.239 g; 1 mM) or **HL₂** (0.245 g; 1 mM) with [NiCl₂(PPh₃)₂] (0.653 g; 1 mM) or [CoCl₂(PPh₃)₂] (0.653 g; 1 mM) in 40 ml of methanol in the presence of methanolic KOH (Scheme 2). The mixture was then continuously refluxed for 5 h. After cooling the solution to room temperature, the precipitate formed was collected by filtration, washed thoroughly with methanol and dried overnight in a vacuum desiccator. The purity of all the complexes was checked by TLC. Micro-analytical data and yield are presented below in this section. Complex **1** dissolved in methanol and chloroform mixture under slow evaporation resulted in the formation of red colored crystals suitable for X-ray diffraction study.

For complex **1**: Yield, 53%. M.p. >250 °C. *Anal. Calc.* for C₂₈H₂₄N₆O₂Ni₁: C, 62.83; H, 4.52; N, 15.70. Found: C, 62.59; H, 4.63; N, 15.79%.

For complex **2**: Yield, 50%. M.p. >250 °C. *Anal. Calc.* for C₂₈H₂₄N₆O₂Co₁: C, 62.75; H, 4.51; N, 15.69. Found: C, 62.89; H, 4.33; N, 15.54%.

For complex **3**: Yield, 51%. M.p. >250 °C. *Anal. Calc.* for C₂₄H₂₀N₆O₂S₂Ni₁: C, 52.67; H, 3.68; N, 15.35; S, 11.72. Found: C, 52.91; H, 3.77; N, 15.22; S, 11.49%.

For complex **4**: Yield, 48%. M.p. >250 °C. *Anal. Calc.* for C₂₄H₂₀N₆O₂S₂Co₁: C, 52.64; H, 3.68; N, 15.34; S, 11.71. Found: C, 52.50; H, 3.76; N, 15.19; S, 11.57%.

2.6. Protein binding studies

Binding of metal hydrazone complexes with bovine serum albumin (BSA) was studied using fluorescence spectra recorded with excitation at 280 nm and corresponding emission at 344 nm assignable to that of bovine serum albumin (BSA). The excitation and emission slit widths and scan rates were constantly maintained for all the experiments. Samples were carefully degassed using pure nitrogen gas for 15 min by using quartz cells (4 × 1 × 1 cm) with high vacuum Teflon stopcocks. Stock solution of BSA was prepared in 50 mM phosphate buffer (pH 7.2) and

stored in the dark at 4 °C for further use. Concentrated stock solutions of the copper complex were prepared by dissolving them in DMSO: phosphate buffer (1:99) and diluted suitably with phosphate buffer to required concentrations. 2.5 ml of BSA solution (1 μ M) was titrated by successive additions of a 2 μ l stock solution of metal hydrazone complexes (10^{-3} M) using a micropipette. Synchronous fluorescence spectra were also recorded using the same concentration of BSA and complexes as mentioned above with two different $\Delta\lambda$ (difference between the excitation and emission wavelengths of BSA) values of 15 and 60 nm.

2.7. Antioxidant activity

2.7.1. Hydroxyl radical scavenging activity

The hydroxyl radical scavenging activity of the compounds was investigated using the Nash method [27]. *In vitro* hydroxyl radicals were generated by Fe^{3+} /ascorbic acid system. The detection of hydroxyl radicals was carried out by measuring the amount of formaldehyde formed from the oxidation reaction with DMSO. The formaldehyde produced was estimated spectrophotometrically at 412 nm. A mixture of 1.0 mL of iron – EDTA solution ferrous ammonium sulfate (0.331 mM) and EDTA (0.698 mM), 0.5 mL of EDTA solution (0.048 mM) and 1.0 mL of DMSO (10.83 mM) (v/v) in 0.1 M phosphate buffer, pH 7.4) sequentially added with solution of test compounds with different concentrations in the test tubes. The reaction was initiated by adding 0.5 mL of ascorbic acid (1.25 mM) and incubated at 80–90 °C for 15 min in a water bath. After incubation, the reaction was terminated by the addition of 1.0 mL of ice-cold TCA (107 mM). Subsequently, 3.0 mL of Nash reagent was added to each tube and left at room temperature for 15 min. The reaction mixture without sample was used as control. The intensity of the color formed was measured spectrophotometrically at 412 nm against reagent blank. The IC_{50} values of the samples were also calculated.

2.7.2. Nitric oxide radical scavenging activity

Nitric oxide scavenging activity was determined based on the reported method [28], where sodium nitroprusside in aqueous solution at physiological pH spontaneously generates nitric oxide, which interacts with oxygen to produce nitrite ions that can be estimated using Greiss reagent. Scavengers of nitric oxide compete in this process leading to reduced production of nitrite ions. For the experiment, sodium nitroprusside (10 mM) in phosphate buffered saline was mixed with 100 μ L of test samples of variable concentrations and incubated at room temperature for 150 min. The same reaction mixture without the sample but the equivalent amount of the solvent served as the control. After the incubation period, 0.5 mL of Griess reagent containing sulfanilamide (5.8 mM), H_3PO_4 (20 mM) and *N*-(1-naphthyl) ethylenediamine dihydrochloride (0.39 mM) was added. The absorbance of the chromophore formed was measured at 546 nm.

2.7.3. Lipid peroxidation

The lipid peroxidation was evaluated by the modified method of Draper and Hadley [29], 1990 *in ex vivo*. Rat liver was cut into small species and stored in deep freezer. One gram of liver was homogenized with 10 ml of saline buffer. From that, 200 μ L of homogenate was taken and added with 100 μ L of test compounds with different concentrations and 50 μ L of 0.07 M FeSO_4 . The content was incubated for 30 min at 37 °C and sequentially added with 1.5 ml of acetic acid (198.5 mM), 1.5 ml of thiobarbituric acid (8 mM) and 50 μ L of trichloroacetic acid (0.2 mM), respectively. The reaction mixture was further incubated in boiling water bath for 60 min and allowed to cool at room temperature and added with 5 ml of butanol. Then the contents were centrifuged and supernatant was collected and read at 532 nm.

For the above three assays, all the tests were run in triplicate and various concentrations of the ligands and their complexes were used to fix a concentration at which the test compounds showed in and around 50% of activity. In addition, the percentage of activity was calculated using the formula, % of activity = $[(A_0 - A_c)/A_0] \times 100$. A_0 and A_c are the absorbance in the absence and presence of the tested compounds, respectively. The 50% of activity (IC_{50}) can be calculated using the percentage of activity results.

2.8. Antimicrobial activity

The *in vitro* antibacterial and antifungal screening of the hydrazone ligands (**HL₁**) and (**HL₂**) and their corresponding metal hydrazone complexes **1**, **2**, **3** and **4** have been carried out against human pathogenic gram positive bacteria (*Staphylococcus aureus* and *Enterococcus faecalis*) and gram negative bacteria (*Klebsiella pneumoniae*, *Escherichia coli* and *Salmonella typhium*) and fungi (*Trichophyton rubrum*, *Candida albicans* (yeast like)) using disc diffusion method [30]. The bacterial and fungal strain were inoculated into the nutrient agar broth and sabouraud dextrose agar broth and incubated for 24 and 48 h, respectively in petriplates. In the disc diffusion method, sterile nutrient agar for bacteria and potato dextrose agar medium for fungi were separately inoculated with the test microorganisms. The compounds to be tested were dissolved in DMSO to a final concentration of 2.5, 5.0 and 7.5 mM and soaked in filter paper disc of 5 mm diameter and 1 mm thickness. The plates were incubated at 32 °C for bacteria (18–24 h) and at 25 °C for fungus (72 h). The diameter (mm) of inhibition zone around each disc was determined after 24 h (bacteria) and 48 h (fungus). Triplicate plates were maintained in both the assays. Streptomycin and Nystatin were used as standards for antibacterial and antifungal studies respectively.

3. Results and discussion

In this study, we treated the respective metal precursor complexes and the heterocyclic hydrazone ligands in 1:1 molar ratio (Scheme 2) with the following expectations that these hydrazones could behave as

- (i) A uninegative bidentate N,O chelating system to yield a four coordinated complex (pathway 1), or
- (ii) A uninegative tridentate chelating system through N,N,O donor atoms to form yet another type of four coordinated complex (pathway 2), or
- (iii) An unusual neutral tridentate N,N,O chelating system to yield a five coordinated metal hydrazone complex with two chloride ions for charge compensation (pathway 3).

Unexpectedly, the heterocyclic hydrazone ligands (**HL₁**) and (**HL₂**) involved in this work deceived all our expectations and formed stable six coordinated metal chelates with 1:2 metal–ligand stoichiometry (pathway 4) without any other side products. The analytical data of all the complexes presented elsewhere in the manuscript also supported the 1:2 compositions.

3.1. Solid structure of the complex $[\text{Ni}(\text{L}_1)_2]$ (**1**)

Molecular structure of $[\text{Ni}(\text{L}_1)_2]$ (**1**) together with the atom labeling scheme is depicted in Fig. 1. The crystallographic data with selected bond lengths and bond angles are listed in Tables 1 and 2. The compound crystallized in monoclinic lattice with space group Cc. Ni(II) center exhibits a distorted octahedral geometry comprising of two equivalent monoanionic ligands coordinated in a

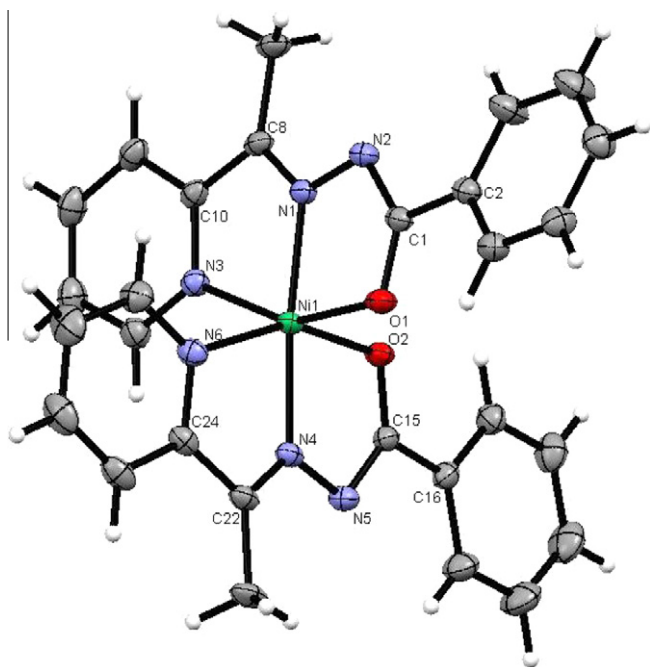


Fig. 1. Molecular structure of complex **1** showing the atom-numbering scheme with ellipsoid of 25% probability.

Table 1
Crystal data and structure refinement data of complex **1**.

Empirical formula	C ₂₈ H ₂₄ N ₆ Ni ₁ O ₂ (1)
Name	[Ni(L ₁) ₂]
Formula weight	535.24
Crystal system	monoclinic
Space group	Cc
Temperature (K)	293(2)
Wavelength (Å)	0.71073
Z	4
<i>Unit cell dimensions</i>	
a (Å)	10.2389(2)
b (Å)	19.6419(6)
c (Å)	12.2648(3)
α (°)	90
β (°)	91.538(10)
γ (°)	90
Color	Red
D _{calc} (Mg/m ³)	1.442
F(000)	1112
Crystal size (mm)	0.22 × 0.20 × 0.17
hkl Limits	−14 ≤ h ≤ 14 −28 ≤ k ≤ 29 −18 ≤ l ≤ 17
θ Range for data collection	2.07° to 32.41°
Reflections collected	7663
R indices (final)	R ₁ = 0.0364, wR ₂ = 0.1036
R indices (all data)	R ₁ = 0.0427, wR ₂ = 0.1077
Goodness-of-fit on F ²	1.046

meridional fashion using *cis* pyridyl nitrogen, *trans* azomethine nitrogen and *cis* enolate oxygen atoms positioned very nearly perpendicular to each other.

The ligand has undergone keto–enol tautomerism and it is well known that the imino tautomers can exist as two geometrical isomers, *syn* (*Z*) and *anti* (*E*), but in this crystal, only the *E* isomer has been observed. The torsion angles C2–C1–N2–N1, −179.5(2)°, N2–N1–C8–C10, −178.2(2)°, C16–C15–N5–N4, −177.6(2)° and N4–C22–C24–C25, 168.8(2)° observed supports the *E* conformation of the ligand on coordination. The coordination around nickel is distorted octahedral with two oxygen atoms and four nitrogen atoms

Table 2
Selected bond lengths (Å) and bond angles (°).

C ₂₈ H ₂₄ N ₆ Ni ₁ O ₂ (1)			
Bond lengths		Bond angles	
Ni1–N1	1.986(2)	O1–Ni1–N1	76.34(7)
Ni1–N3	2.095(2)	N1–Ni1–N3	78.27(7)
Ni1–O1	2.097(2)	O2–Ni1–N4	76.60(7)
Ni1–N6	2.094(2)	N4–Ni1–N6	78.07(8)
Ni1–N4	1.989(2)	O1–Ni1–N3	154.04(7)
Ni1–O2	2.102(2)	O2–Ni1–N6	154.27(7)
C2–C1–N2–N1	−179.5(2)	N4–Ni1–N1	174.24(8)
N2–N1–C8–C10	−178.2(2)	N1–Ni1–N6	105.96(8)
C16–C15–N5–N4	−177.6(2)	N1–Ni1–O2	99.63(7)
N4–C22–C24–C25	168.8(2)	N3–Ni1–N4	106.12(7)
		N4–Ni1–O1	99.58(7)
		O1–Ni1–O2	96.21(7)
		N3–Ni1–N6	89.46(8)

occupy the coordination sites with the ligand–metal–ligand bite angles varying between 78.27(7)° [N3–Ni1–N1], 76.34(7)° [O1–Ni1–N1], 76.60(7)° [O2–Ni1–N4] and 78.07(8)° [N4–Ni1–N6].

The two central coordinating bonds [Ni1–N1] 1.986(2) Å and [Ni1–N4] 1.989(2) Å are comparable to the basal planar bonds [Ni1–O1] 2.097(2) Å, [Ni1–N3] 2.095(2) Å, [Ni1–N6] 2.094(2) Å and [Ni1–O2] 2.102(2) Å confirming that all the bonds in basal plane are almost equal in length but the axial bonds are little longer than that of the former. The [N4–Ni1–N1] trans angle was found as 174.24(8)° but the other trans angles [O1–Ni1–N3] 154.04(7)° and [O2–Ni1–N6] 154.27(7)° are constrained within the meridional ligands. These observations suggested that the coordination geometry around the nickel ion had undergone much distortion from a perfect octahedron. A perspective view of unit cell packing of complex **1** is shown in Fig. 2.

3.2. Infrared spectra

In the absence of a powerful technique such as X-ray crystallography, IR spectra has proven to be the most suitable technique to

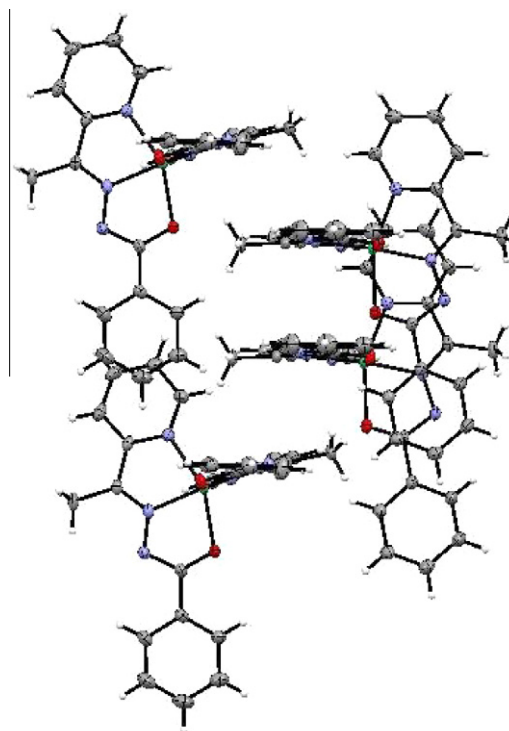


Fig. 2. Packing diagram of the unit cell of complex **1**.

give enough information to elucidate the nature of bonding of the ligands to the metal ions.

IR spectra of the ligands showed characteristic stretching vibrations in the region of 3178 & 3170, 1656 & 1643, 1540 & 1573 and 1060 & 993 cm^{-1} due to $\nu_{(\text{N-H})}$, $\nu_{(\text{C=O})}$, $\nu_{(\text{C=N})}$ and $\nu_{(\text{N-N})}$ vibrations of **HL₁** and **HL₂** ligands, respectively. In the IR spectra of the complexes, we observed the disappearance of bands due to C=O and N-H stretching vibrations and the appearance of new bands attributed to $\nu_{(\text{C-O})}$ and $\nu_{(\text{C=N-N=C-})}$ in the range of 1299–1306 and 1591–1598 cm^{-1} & 1490–1497 cm^{-1} [31], respectively due to enolisation followed by deprotonation prior to coordination. Further, the stretching frequency of C=N slightly shifted to lower wave number, which supports that azomethine nitrogen atoms were coordinated to the central metal atom [32]. In addition, the characteristic $\nu_{(\text{N-N})}$ stretching of the free ligands **HL₁** and **HL₂** (observed at 1060 or 993 cm^{-1}) undergoes a positive shift to a higher wave number upon complexation due to diminished repulsion between the lone pairs of adjacent nitrogen atoms [33–35]. All the above mentioned IR spectral data are summarized in Table 3.

3.3. Electronic spectra

The electronic spectra of the complexes recorded in methanol displayed three to four bands in the region 232–387 nm (Table 4). The bands appeared in 232–309 nm region in the spectra of all the complexes is assigned to the intra-ligand $\pi-\pi^*$ transition due to the formation of conjugated double bond after complexation to the metal ions [36]. In addition to the above absorptions, all the new hydrazone complexes showed another band in the region 367–387 nm aroused out the ligand to metal charge transfer (LMCT) transitions [37] and a representative spectrum for the complex **1** is shown in Fig. 3. The nature and position of the electronic spectral absorptions of all the complexes indicated an octahedral geometry around metal ions in these complexes.

3.3.1. ¹H NMR spectra

¹H NMR spectra of the hydrazone ligands were assigned on the basis of observed chemical shift and relative intensities of the signals. The ¹H NMR spectra of both the ligands **HL₁** and **HL₂** displayed sharp singlets owing to the -NH protons and the methyl protons of -CH₃-C=N at 9.07 or 9.38 ppm and at 2.48 or 2.53 ppm respectively. The signals corresponding to the protons of respective benzoyl, thiophene and pyridyl moieties were observed as multiplets in the range of 7–8 ppm. A representative spectrum for the **HL₂** ligand is shown in Fig. 4. All these observations supported the structure of the ligands assigned on the basis of infrared vibrations.

3.4. Emission spectra

Synthesis of coordination complexes using functional ligands and transition-metal centers can be a useful method to obtain

Table 3
IR spectral frequencies of the free ligand and its metal(II) complexes.

Ligand/complex	$\nu_{(\text{N-H})}$	$\nu_{(\text{C=O})}$	$\nu_{(\text{C=N})}$	$\nu_{(\text{C-O})}$	$\nu_{(\text{N-N})}$
HL₁	3178	1656	1540		1060
1			1593	1299	1099
			1496		
2			1591	1301	1098
			1491		
HL₂	3170	1643	1573	1298	993
3			1596	1300	1029
			1497		
4			1598	1306	1028
			1490		

ν in cm^{-1} .

Table 4
Characteristic electronic and emission spectral data.

Complex	λ_{max} (nm)	Emission ^c data (λ_{max} (nm))
1	370 ^a , 289 ^b , 248 ^b	496
2	354 ^a , 281 ^b , 232 ^b	461
3	387 ^a , 309 ^b , 268 ^b , 241 ^b	447
4	368 ^a , 267 ^b , 243 ^b	416

^a LMCT.

^b ILCT.

^c Excitation at LMCT.

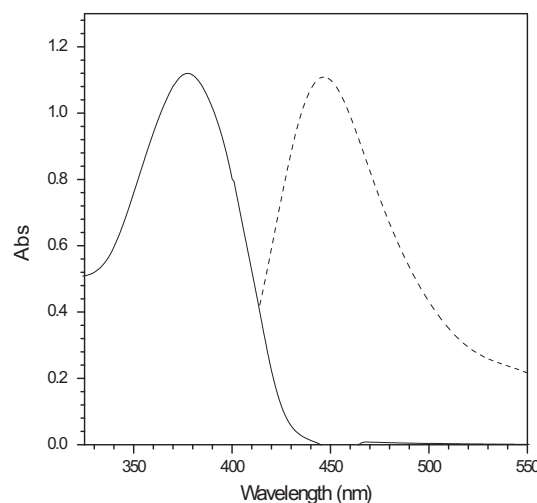


Fig. 3. Absorption (---) and emission (—) spectra of complex **1**.

new photoluminescent materials. Emission properties of the metal hydrazone complexes in methanol were examined at room temperature. When an excitation wavelength corresponding to the lowest energy absorption was used, no emission band was observed. However, when the samples are excited using higher wavelength, all the complexes showed strong emission. The emission maxima of the complexes were observed in the 416–496 nm range and are listed in Table 4 and a representative spectrum for the complex **1** is shown in Fig. 3 (dashed line). The wavelength of emission maxima of all the complexes have experienced a positive shift of about 48–126 nm compared to those of excitation maxima. The observed CT luminescence in these complexes may be due to the presence of imine functional group. The luminescence observed in these complexes are a molecular property, attributed to the $\pi-\pi^*$ transition of the *N*-arylmethylenebenzhydrazones [38].

3.5. Electrochemical studies

Electrochemical properties of the ligands **HL₁** and **HL₂** and corresponding metal complexes **1–4** were studied in methanol with tetrabutylammonium perchlorate as supporting electrolyte at a scan rate of 100 mV s^{-1} . The ligands used in this work were not reversibly reduced or oxidized in the potential range applied, hence the observed redox process were assigned to the metal centered only. The cyclic voltammogram of the complex **1** showed the peaks at +0.8965 and +0.8024 V was shown in Fig. 5 (Table 5). Anodic response obtained at +0.8965 V is believed to be due to Ni(II) → Ni(III) oxidation and the cathodic response at +0.8024 V is due to the Ni(III) → Ni(II) reduction. The peak-to-peak separation value ($\Delta E_p = 94 \text{ mV}$) and the ratio of i_c/i_a due to cathodic and anodic sweeps at different scan rates (25–200 mV s^{-1}) revealed that this process can be at best as reversible oxidation. The

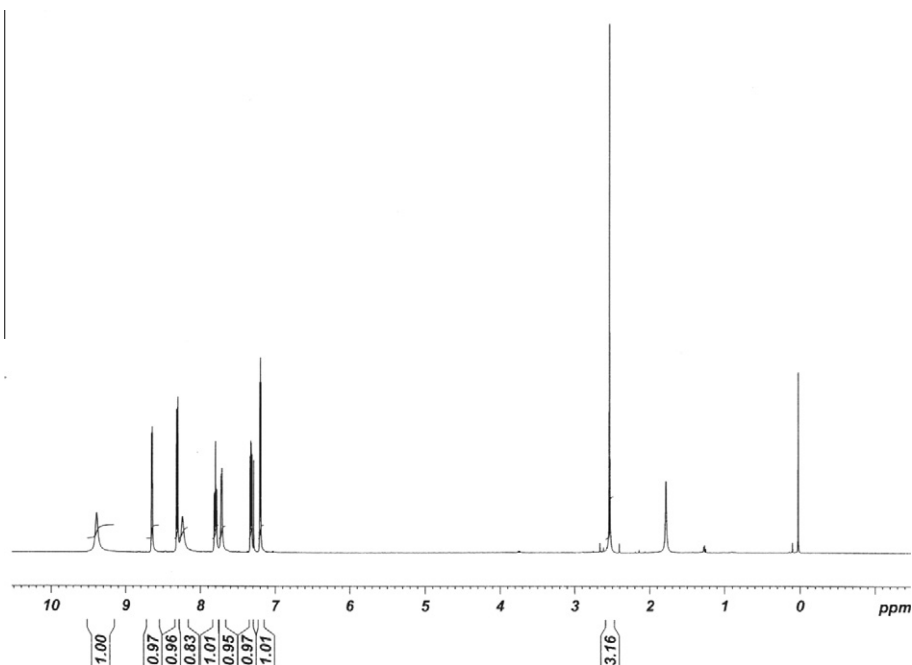


Fig. 4. ^1H NMR spectrum of the hydrazone ligand **HL**₂.

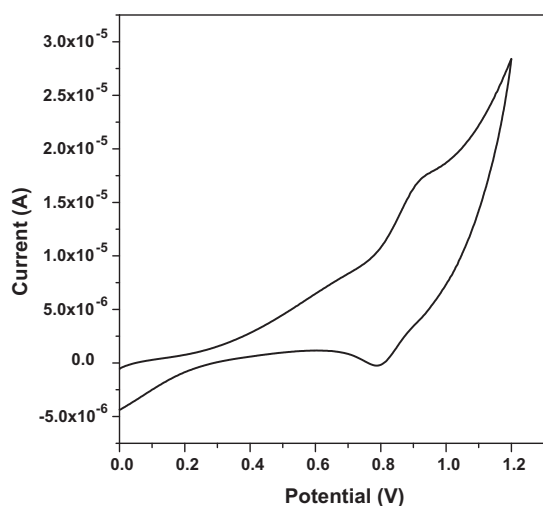


Fig. 5. Cyclic voltammogram of complex **1**.

Table 5
Cyclic voltammetric data of metal hydrazone complexes.

Complex	M(III)–M(II)			
	E_{pa} (V)	E_{pc} (V)	$E_{1/2}$ (V)	ΔE_{p} (mV)
1	0.8965	0.8024	0.8495	94
2	0.6846	0.1153	0.4000	569
3	0.8456	0.1030	0.4740	743
4	0.8141	0.1773	0.4957	636

Supporting electrolyte: NBu_4ClO_4 ; solvent: MeOH; $\Delta E_{\text{p}} = E_{\text{pa}} - E_{\text{pc}}$, where E_{pa} and E_{pc} are anodic and cathodic potentials respectively; $E_{1/2} = 0.5(E_{\text{pa}} + E_{\text{pc}})$; scan rate: 100 mV s^{-1} .

voltammogram of the complexes **2**, **3** and **4** showed anodic peaks at +0.6846, +0.8456 and +0.8141 V, respectively attributed to the oxidation of $\text{M(II)} \rightarrow \text{M(III)}$ with a corresponding reduction peak of $\text{M(III)} \rightarrow \text{M(II)}$ at +0.1153, +0.1030 and +0.1773 V with a peak to peak separation (ΔE_{p}) of 569, 743 and 636 mV, respectively.

The higher magnitude of ΔE_{p} as well as its increase while increasing the scan rate confirmed that the electrochemical process is a quasi-reversible oxidation attributed to the slow electron transfer and adsorption of the complexes on to the electrode surface.

3.6. Protein binding studies

3.6.1. Fluorescence spectroscopy

Qualitative analysis of binding of chemical compounds to BSA can be detected by examining fluorescence spectra. Generally, the fluorescence of protein is caused by three intrinsic characteristics of the protein, namely tryptophan, tyrosine and phenyl alanine residues. Fluorescence quenching refers to any process that decreases the fluorescence intensity from a fluorophore due to variety of molecular interactions including excited-state reactions, molecular rearrangements, energy transfer ground-state complex formation and collisional quenching. Here, the change in fluorescence intensity is related to both the concentration and nature of the quencher. Therefore, the quenched fluorophore serves as an indicator to determine the ability of quenching agent. It is obvious that BSA has a strong fluorescence emission peaked at 344 nm. When BSA was titrated with different amounts of metal hydrazone complexes, a remarkable intrinsic fluorescence decrease of the protein was observed with a hypsochromism of about 3, 10, 4 and 15 nm respectively for complexes **1**, **2**, **3** and **4** (Fig. 6). Fluorescence quenching is described by the Stern-Volmer equation [39]: $I_0/I = 1 + K_{\text{SV}} [Q]$; where I_0 and I represent the fluorescence intensities in the absence and presence of quencher, respectively. K_{SV} is the Stern-Volmer quenching constant and $[Q]$ is the quencher concentration. K_{SV} value obtained from the plot of I_0/I vs $[Q]$ was found to be 1.6506×10^5 , 1.9323×10^5 , 2.3203×10^5 and $4.8025 \times 10^5 \text{ M}^{-1}$, corresponding to the respective metal hydrazone chelates **1**, **2**, **3** and **4** (Fig. 6).

3.6.2. Absorption spectral studies

UV–Vis absorption measurement is a simple but effective method to detect complex formation in solution phase. Quenching can occur by different mechanisms either by dynamic or static. Dynamic quenching refers to a process in which the fluorophore

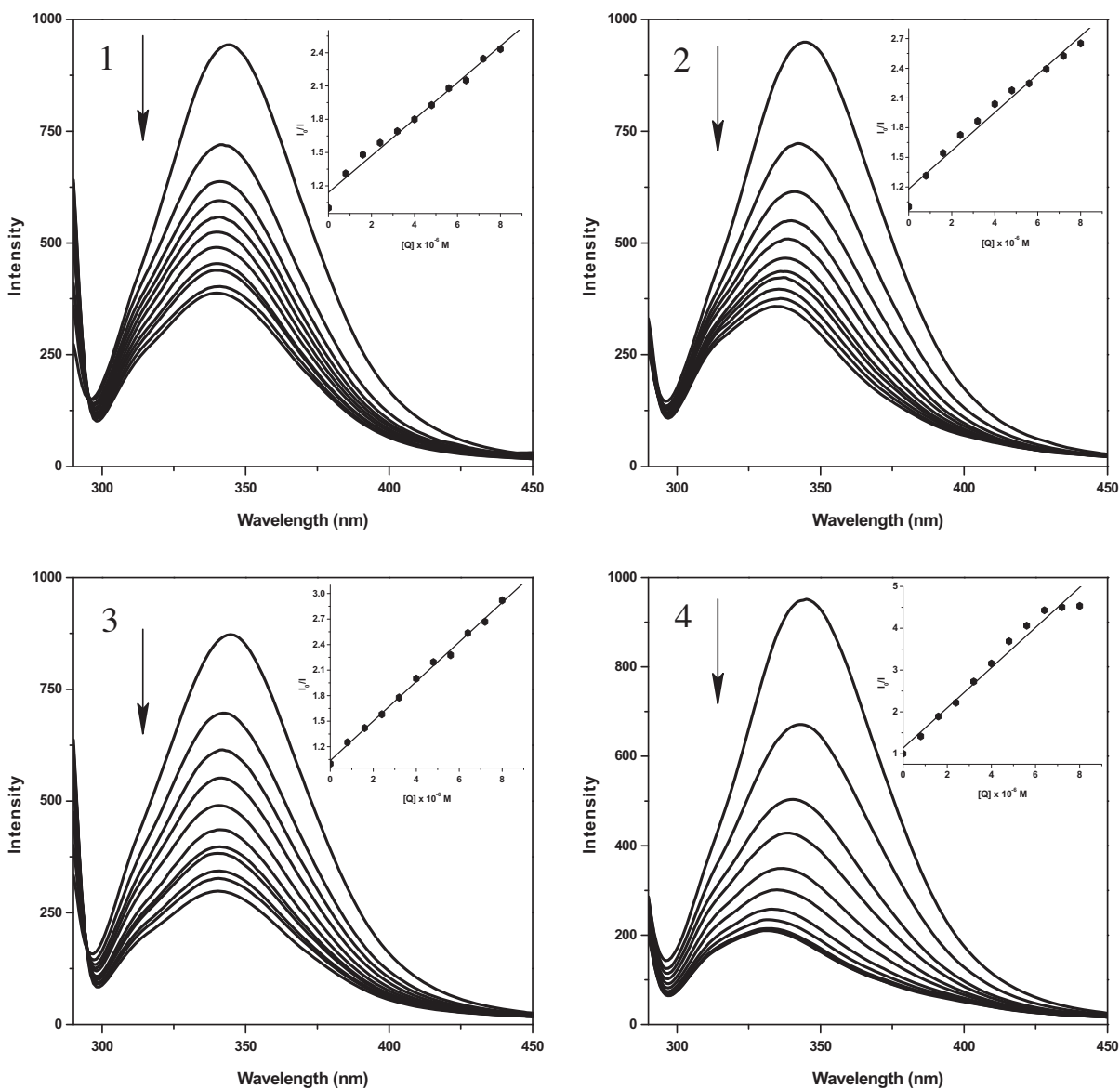


Fig. 6. Emission spectrum of BSA (1×10^{-6} M; $\lambda_{\text{exi}} = 280$ nm; $\lambda_{\text{emi}} = 344$ nm) as a function of concentration of the complexes **1**, **2**, **3** and **4** (0.8 , 1.6 , 2.4 , 3.2 , 4.0 , 4.8 , 5.6 , 6.4 , 7.2 and 8.0×10^{-6} M). Arrow indicates the effect of metal complexes on the fluorescence emission of BSA. (Inset: Stern-Volmer plot of the fluorescence titration data corresponding to the complex **1**, **2**, **3** and **4**).

and the quencher come into contact during the transient existence of the excited state while the later type of quenching refers to fluorophore–quencher complex formation in the ground state. In order to validate the quenching mechanism, the absorption spectra of BSA in the absence and presence of hydrazone complexes were determined. After the addition of appropriate amount of hydrazone complexes **1**, **2**, **3** and **4** to BSA resulted in an increase in the intensity of absorption band of BSA observed at 278 nm suggesting that an interaction between metal hydrazones and BSA occurred and the possible quenching mechanism of fluorescence of BSA by these chelates is a static one [40]. A representative absorption spectrum of pure BSA and BSA-complex **4** is shown in Fig. 7.

3.6.3. Binding constants and the number of binding sites

For the static quenching interaction, if it is assumed that there are similar and independent binding sites in the biomolecule, the binding efficiency of the test compounds with the BSA can be determined according to the method described by using the following equation [41]: $\log [(F_0 - F)/F] = \log [K] + n \log [Q]$, where,

in the present case, K is the binding constant for the metal hydrazones–BSA and n is the number of binding sites per albumin molecule, which can be determined from the slope and the intercept of the double logarithm regression curve of $\log [(F_0 - F)/F]$ versus $\log [\text{complex}]$ based on the above equation. Binding constants obtained from the plot of $\log [(F_0 - F)/F]$ versus $\log [Q]$ (Fig. 8) corresponding to complexes **1**, **2**, **3** and **4** were calculated to be 3.064×10^3 , 6.4969×10^4 , 6.628×10^4 and 3.3768×10^5 M $^{-1}$, respectively.

3.6.4. Synchronous measurements

Influence of metal chelates on the conformational changes of BSA was assessed by synchronous fluorescence spectra. Synchronous fluorescence measurements provide information about the molecular micro-environment in the vicinity of the functional fluorophore groups [42]. Synchronous fluorescence spectra are obtained by simultaneously scanning excitation and emission monochromators. As $\Delta\lambda$ between excitation wavelength and emission wavelength is 15 nm, synchronous fluorescence offers characteristics of tyrosine residues, while with $\Delta\lambda$ as 60 nm, it provides

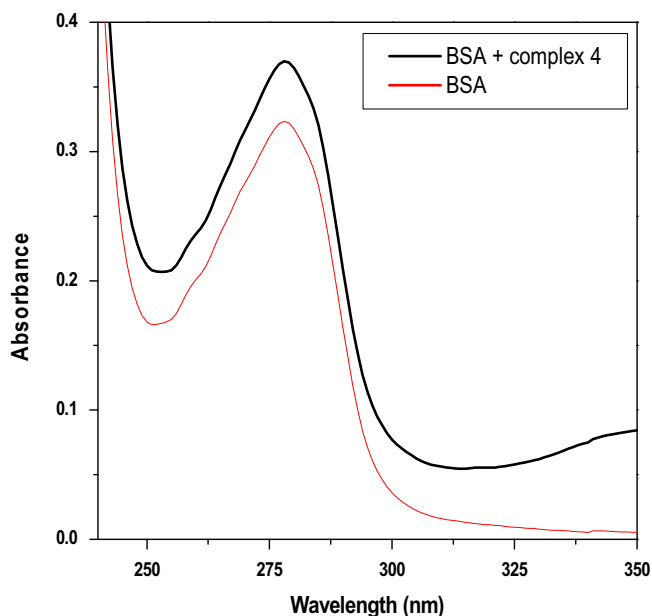


Fig. 7. The absorption spectra of BSA (1×10^{-5} M) and BSA-complex 4 (BSA = 1×10^{-5} M and complex 4 = 1×10^{-6} M).

the characteristic information of tryptophan residues [43]. The changes in maximum emission position correspond to the change in the polarity around the chromophore molecule. Thus, the environment of amino acid residues can be studied by measuring the shift in wavelength of emission maximum. The synchronous fluorescence spectroscopy of BSA upon addition of metal chelates gained at $\Delta\lambda = 15$ nm and $\Delta\lambda = 60$ nm are shown in Figs. 9–12.

It appears from Figs. 9A, 10A, 11A and 12A that the emission intensity corresponding to tyrosine residue increases with a red shift of 1 nm in the case of interaction with complex 1 whereas the same band showed a decrease in the intensity of emission without any wavelength shift upon interaction with complex 2. However, in case of complexes 3 and 4, a decrease in emission intensity with a red shift of about 1 nm was observed. Regarding the changes in the emission intensity due to tryptophan residues upon interaction with the above said complexes, a gradual de-

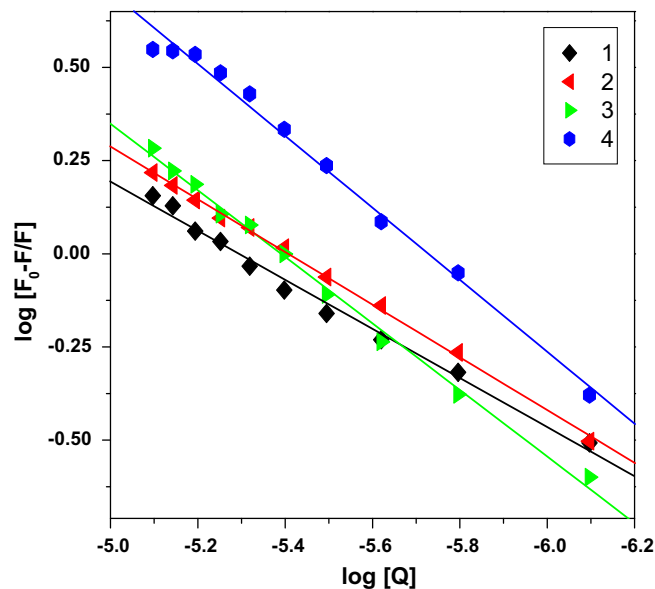


Fig. 8. Plot of $\log [(F_0 - F)/F]$ vs $\log [Q]$ for complexes 1, 2, 3 and 4.

crease in the fluorescence intensity with a blue shift was observed in case of complexes 2, 3 and 4 but only a decrease in intensity without any shift corresponding to complex 1 (Figs. 9B, 10B, 11B and 12B). These results suggest that the hydrazones did influence the micro-environment around both tyrosine and tryptophan residues of BSA as observed with other hydrazone complexes [26].

3.7. Antioxidant studies

3.7.1. Hydroxyl radical scavenging activity

Hydroxyl radical is highly reactive oxygen centered radical formed from the reactions of various hydroperoxides with transition metal ions. Among all the free radicals, hydroxyl radical is by far the most potent and therefore the most dangerous oxygen metabolite and hence the elimination of this radical is one of the major aims of antioxidant administration [44]. It attacks

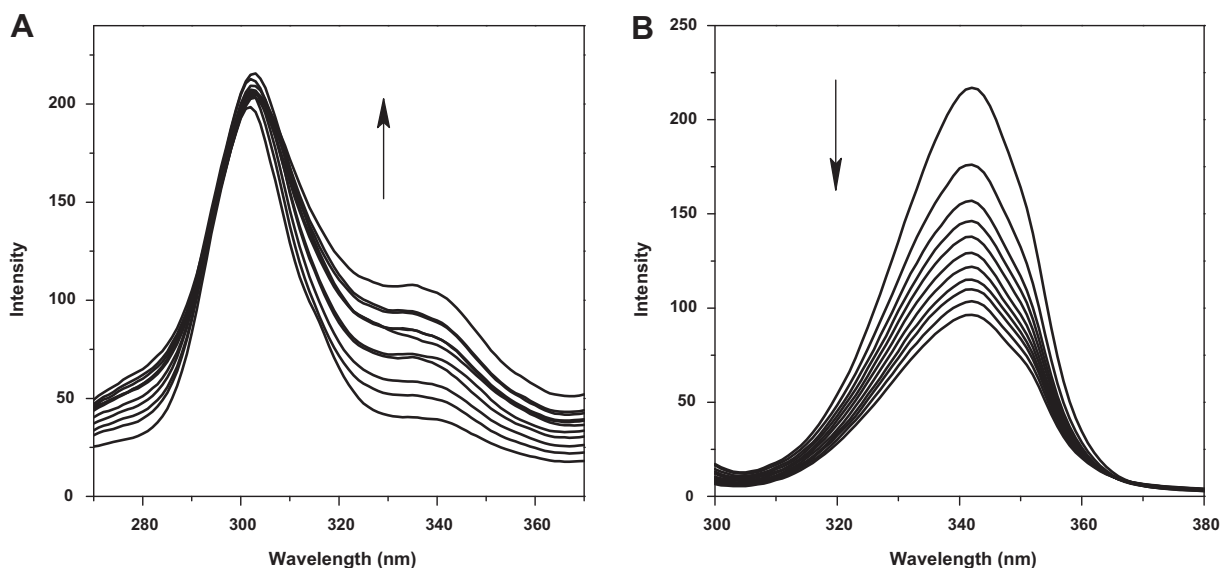


Fig. 9. Synchronous spectra of BSA (1×10^{-6} M) as a function of concentration of the complex 1 ($0.8, 1.6, 2.4, 3.2, 4.0, 4.8, 5.6, 6.4, 7.2$ and 8.0×10^{-6} M) with wavelength difference of $\Delta\lambda = 15$ nm (A) and $\Delta\lambda = 60$ nm (B). Arrow indicates the change in emission intensity w.r.t various concentration of complex 1.

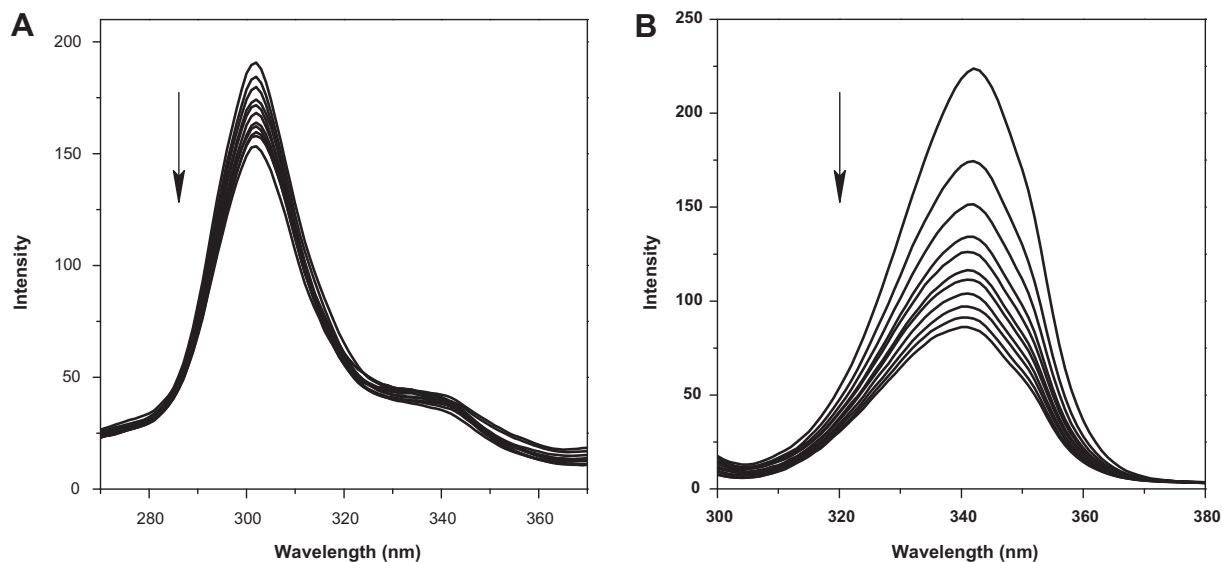


Fig. 10. Synchronous spectra of BSA (1×10^{-6} M) as a function of concentration of the complex **2** ($0.8, 1.6, 2.4, 3.2, 4.0, 4.8, 5.6, 6.4, 7.2$ and 8.0×10^{-6} M) with wavelength difference of $\Delta\lambda = 15$ nm (A) and $\Delta\lambda = 60$ nm (B). Arrow indicates the change in emission intensity w.r.t various concentration of complex **2**.

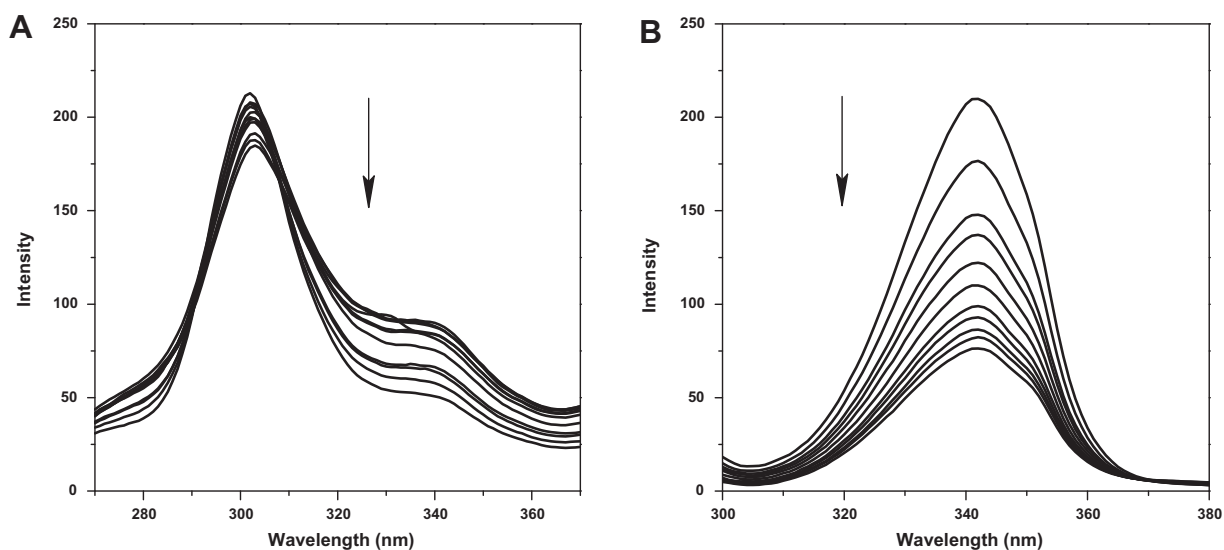


Fig. 11. Synchronous spectra of BSA (1×10^{-6} M) as a function of concentration of the complex **3** ($0.8, 1.6, 2.4, 3.2, 4.0, 4.8, 5.6, 6.4, 7.2$ and 8.0×10^{-6} M) with wavelength difference of $\Delta\lambda = 15$ nm (A) and $\Delta\lambda = 60$ nm (B). Arrow indicates the change in emission intensity w.r.t various concentration of complex **3**.

proteins, DNA, polyunsaturated fatty acid in membranes and most biological molecules [45]. Hydroxyl radical is known to be capable of abstracting hydrogen atoms from membrane lipids and brings about peroxidic reaction of lipids. Scavenging activity of the free ligands and corresponding metal hydrazones on hydroxyl radical has been investigated and their inhibitory effect on $\cdot\text{OH}$ is shown in Fig. 13. By comparing the antioxidant activity of the ligands (IC_{50} value for **HL**₁ and **HL**₂ are 166.25 and 121.30 μM , respectively) with that of the metal complexes (IC_{50} values of **1**, **2**, **3** and **4** are 35.26, 29.88, 31.70 and 25.28 μM , respectively) it became clear that the metal complexes possess higher scavenging activity towards $\cdot\text{OH}$ than the respective parent ligands. Among all the complexes, complexes **3** and **4** showed more scavenging potential than the rest of the metal hydrazone complexes, which may be due to the presence of thiophene moiety in the former. However, among the complexes

containing thiophene moiety in their molecular architecture, the one containing cobalt ion as the metal center (complex **4**) showed very high activity than that of nickel ion under identical experimental conditions.

3.7.2. Nitric oxide radical scavenging activity

Nitric oxide (NO) is a diffusible free radical which plays many role as an effectors in diverse biological systems including neuronal messenger, vasodilation, antimicrobial and antitumor activities [46]. Nitric oxide inhibitors were shown to have beneficial effects on some aspect of inflammation and tissue damage seen in inflammatory diseases [47]. In order to understand the ability of the hydrazone ligands and their corresponding metal complexes towards the reactive radical species, NO scavenging assay of them was carried in various concentrations and the results are presented in Fig. 13 with the corresponding IC_{50} values of the ligands **HL**₁ and

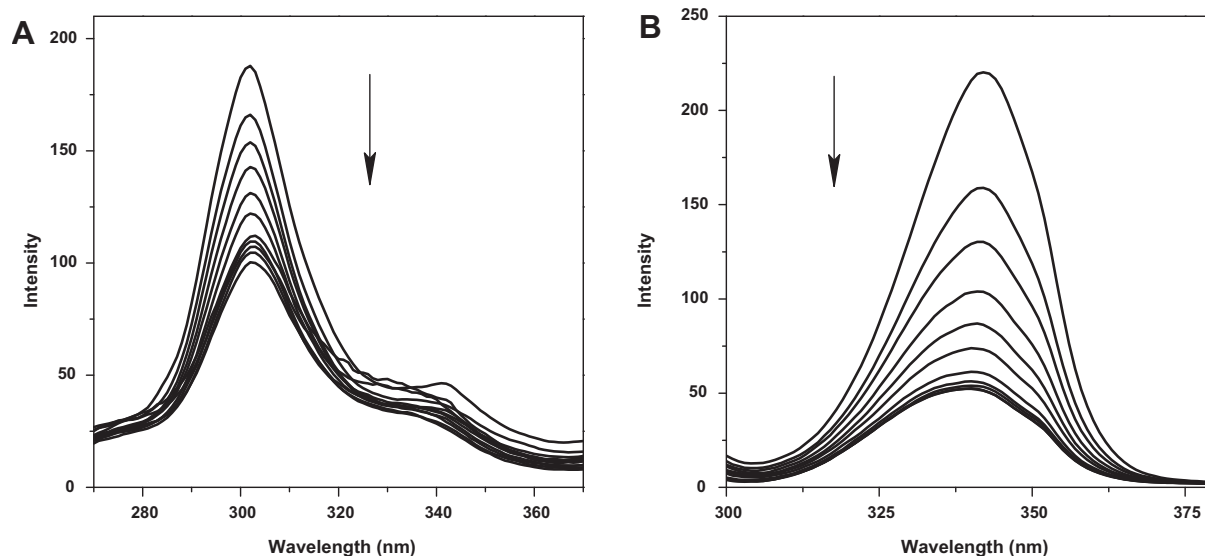


Fig. 12. Synchronous spectra of BSA (1×10^{-6} M) as a function of concentration of the complex **4** ($0.8, 1.6, 2.4, 3.2, 4.0, 4.8, 5.6, 6.4, 7.2$ and 8.0×10^{-6} M) with wavelength difference of $\Delta\lambda = 15$ nm (A) and $\Delta\lambda = 60$ nm (B). Arrow indicates the change in emission intensity w.r.t various concentration of complex **4**.

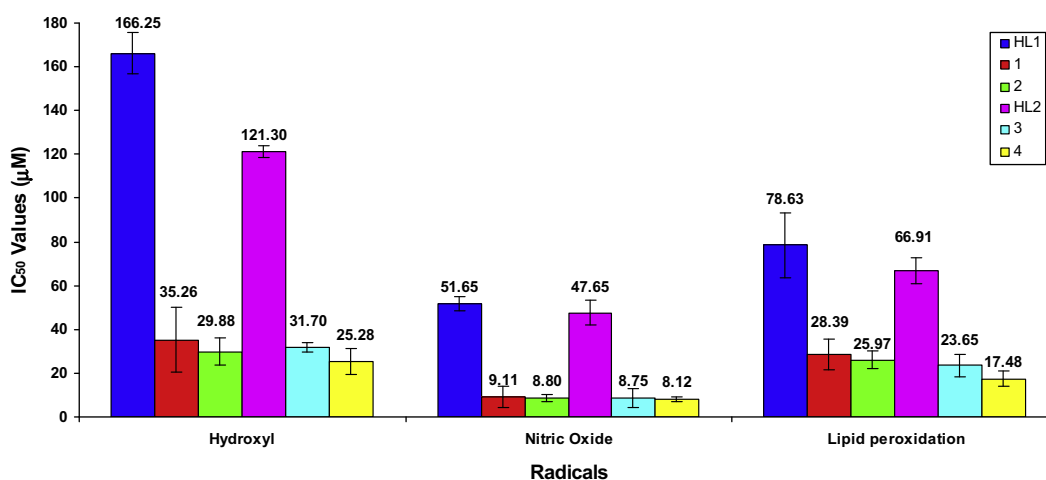


Fig. 13. Trends in the inhibition of hydroxyl, nitric oxide and lipid peroxidation radicals by the hydrazone ligands and corresponding metal complexes.

HL₂ (IC_{50} values are 51.65 and 47.65 μ M) and the metal complexes **1**, **2**, **3** and **4** (IC_{50} values are 9.11, 8.80, 8.75 and 8.12 μ M). However, the results indicated that the metal complexes exhibited greater antioxidant activity than the free ligands **HL₁** and **HL₂**. Among the tested complexes, complex **4** displayed high scavenging activity due to the presence of thiophene moiety and Co(II) ion as described in the previous section.

3.7.3. Lipid peroxidation assay

The mechanisms involved in many human diseases such as hepato toxicities, hepatocarcinogenesis, diabetes, malaria, acute myocardial infarction, skin cancer include lipid peroxidation as a main source of membrane damage [48]. Lipid peroxidation was assessed as formation of lipid hydroperoxides and TBARS. In order to examine the possible mechanisms of action we have studied the abilities of **HL₁**, **HL₂**, **1**, **2**, **3** and **4** to prevent oxidative damage of rat liver. The inhibition of lipid peroxidation by **HL₁**, **HL₂**, **1**, **2**, **3** and **4** (the IC_{50} values are 78.63, 66.91, 28.39, 25.97, 23.65 and 17.48 μ M, respectively) is displayed in Fig. 13. Overall, the results demonstrate that the complex **4** has a greater capacity to prevent oxidative deterioration of lipids than **HL₁**, **HL₂**, **1**, **2** and **3**. Among the tested complexes, complex **4** displayed

high scavenging activity due to the presence of thiophene moiety and Co(II) ion as described in the previous section reports. All the test compounds compared with the standard compound butylated hydroxy anisole (BHA) showed superior activity in all the analysis. However, the results indicated that the metal complexes exhibited greater antioxidant activity than the free ligands **HL₁** and **HL₂**.

In general, the antioxidant activity of the ligands **HL₁**, **HL₂** and its M(II) complexes [where M = Ni or Co] against the free radicals i.e., OH, NO and lipid peroxidation was found to decrease in the order of **4** > **3** > **2** > **1** > **HL₂** > **HL₁** in these experiments. Further, the results obtained against the different radicals confirmed that the complexes are more effective to arrest the formation of the nitric oxide than the rest of the radicals. The observed lower IC_{50} values in antioxidant assays did demonstrate that these complexes have the potential as drugs to eliminate the radicals.

3.8. Antimicrobial studies

Some important factors such as the nature of metal ion, nature of the ligand, coordinating sites, geometry of the complex,

Table 6
Antibacterial activity data of hydrazone ligands and corresponding metal complexes.

Ligand/ complex	Diameter of inhibition zone ^a (mm)															
	<i>S. aureus</i>			<i>K. pneumoniae</i>			<i>E. coli</i>			<i>S. typhium</i>			<i>E. faecalis</i>			
	2.5 mM	5 mM	7.5 mM	2.5 mM	5 mM	7.5 mM	2.5 mM	5 mM	7.5 mM	2.5 mM	5 mM	7.5 mM	2.5 mM	5 mM	7.5 mM	
HL₁					3 ± 0.7	5 ± 0.3				5 ± 0.4						
1		9 ± 0.4	10 ± 0.3	7 ± 0.7	10 ± 0.9	14 ± 0.5	8 ± 0.3	14 ± 0.2	18 ± 0.8				9 ± 0.7	10 ± 0.2	13 ± 0.8	16 ± 0.7
2	5 ± 0.2	12 ± 0.9	14 ± 0.8	9 ± 0.4	14 ± 0.6	17 ± 1.1	10 ± 0.5	12 ± 0.4	18 ± 1.2		9 ± 0.5	16 ± 0.5	10 ± 0.3	15 ± 0.4	20 ± 0.7	
HL₂			5 ± 0.6		4 ± 0.7	7 ± 0.5			7 ± 0.9					5 ± 1.1	8 ± 0.2	
3	4 ± 0.8	11 ± 0.8	14 ± 0.4	8 ± 0.3	13 ± 1.2	19 ± 0.9	9 ± 0.7	15 ± 0.2	20 ± 0.5	7 ± 0.7	11 ± 0.4	15 ± 0.4	13 ± 0.7	18 ± 0.9	22 ± 0.6	
4	7 ± 0.5	12 ± 0.7	16 ± 0.4	8 ± 0.5	14 ± 0.9	19 ± 0.4	10 ± 0.7	17 ± 0.7	23 ± 0.2	5 ± 0.5	11 ± 0.8	18 ± 1.2	15 ± 0.3	16 ± 0.6	25 ± 0.4	
S	11 ± 1.1	16 ± 1.5	21 ± 0.9	10 ± 0.5	16 ± 0.7	23 ± 0.8	13 ± 0.6	19 ± 0.9	27 ± 0.8	11 ± 0.4	18 ± 0.5	25 ± 0.5	14 ± 0.8	21 ± 0.7	29 ± 0.9	

S = Streptomycin.

^a Average of triplicates.**Table 7**
Antifungal activity data of hydrazone ligands and corresponding metal complexes.

Ligand/ complex	Diameter of inhibition zone ^a (mm)					
	<i>Trichophyton rubrum</i>			<i>Candida albicans</i>		
	2.5 mM	5 mM	7.5 mM	2.5 mM	5 mM	7.5 mM
HL₁		6 ± 0.6	6 ± 1.1			
1	5 ± 0.7	11 ± 0.7	15 ± 0.4		8 ± 0.3	13 ± 0.5
2	5 ± 0.2	14 ± 0.4	19 ± 0.9		11 ± 0.5	16 ± 0.7
HL₂		9 ± 0.4	13 ± 0.7			5 ± 0.9
3	8 ± 0.4	17 ± 0.5	22 ± 0.2	5 ± 0.4	13 ± 0.3	16 ± 0.7
4	8 ± 0.3	19 ± 0.8	25 ± 0.3	5 ± 0.7	14 ± 0.2	18 ± 0.2
S	13 ± 0.7	21 ± 0.3	30 ± 1.2	11 ± 0.9	18 ± 0.8	24 ± 0.4

S = Nystatin.

^a Average of triplicates.

concentration, hydrophilicity and lipophilicity have considerable influence on antibacterial activity. Certainly, steric and pharmacokinetic factors also play a decisive role in deciding the potency of an antimicrobial agent. Heterocyclic ligands with multifunctional groups have a greater chance of interaction either with nucleoside bases (even after complexation with metal ion) or with biologically essential metal ions present in the biosystem and can be promising candidates as bactericides [49]. Thus antibacterial property of metal complexes cannot be ascribed to chelation alone, but it is an intricate blend of several contributions.

The results of antibacterial studies of the free ligands and their corresponding Ni(II) and Co(II) complexes were given in Table 6. From the data presented in the table, it is clear that the metal complexes **1–4** were more active than the ligands **HL₁** and **HL₂**.

The antifungal activity of the free hydrazone ligand showed a considerable enhancement upon coordination with the metal ions against the same fungal strains. In our study, both the hydrazone ligands did not show any activity against *Trichophyton rubrum* and *Candida albicans* at all experimental concentrations. However, the metal complexes derived from them showed significant antifungal activity against *Trichophyton rubrum* and *Candida albicans* (Table 7). It was evident from the data that this activity significantly increased upon coordination that can be rationalized on the basis that their structures mainly possess an additional C=N bond due to enolisation during chelate formation. Among all the complexes, the complex **4** possessed very high activity due to the presence of thiophene moiety and biologically essential metal ion, Co(II) ion. Moreover, coordination reduces the polarity [50,51] of the metal ion mainly because of the partial sharing of its positive charge with the donor groups [52] within the chelate ring system formed during coordination. This process, in turn, increases the lipophilic nature of the central metal atom, which favors its permeation more efficiently through the lipid layer of the microorganism [53,54] thus destroying them more aggressively. However, the antimicrobial activity of the tested ligands and com-

plexes is only very modest and also they could not reach the effectiveness of standard antimicrobial drugs such as streptomycin and nystatin.

4. Conclusion

Four new octahedral Ni(II) and Co(II) complexes of heterocyclic hydrazone ligands were synthesised and characterized by various spectral data. All the complexes were found to have the metal to ligand molar ratio of 1:2 instead of the expected 1:1 composition. The single crystal X-ray crystallographic study of complex **1** revealed the distorted octahedral configuration around the metal ion. The interaction between metal chelates and BSA in buffer solution studied by UV–Vis, fluorescence and synchronous fluorescence spectroscopic methods did suggest that the metal hydrazone chelates possess strong ability to quench the BSA fluorescence mainly through a static quenching process. The results of synchronous fluorescence measurements revealed that the present metal hydrazone chelates did influence the micro-environment around both tyrosine and tryptophan residues of BSA. The results of antioxidant and antimicrobial studies revealed that the metal complexes are more effective than that of the respective free ligands under identical experimental conditions. Among the four different complexes synthesised, complex **4** containing thiophene moiety in the ligand compartment with cobalt ion as the metal center showed higher activity than the corresponding nickel counter part with respect to all kinds of studies undertaken in the present work.

Acknowledgement

We sincerely thank Dr. S. Abraham John, Gandhigram University, Gandhigram, India for carrying out the electrochemical measurements. We are also grateful to Department of Science and Technology (DST) for the award of Senior Research Fellowship (SRF) to P. Sathyadevi. PTM is thankful to DST-India (FIST Programme at School of Chemistry, Bharathidasan University) for the use of Bruker Smart APEX II diffractometer.

Appendix A. Supplementary data

CCDC 771884 contains the supplementary crystallographic data for this paper. These data can be obtained free of charge via <http://www.ccdc.cam.ac.uk/conts/retrieving.html>, or from the Cambridge Crystallographic Data Centre, 12 Union Road, Cambridge CB2 1EZ, UK; fax: +44 1223 336 033; or e-mail: deposit@ccdc.cam.ac.uk.

Reference

- [1] N. Wang, L. Ye, B.Q. Zhao, J.X. Yu, Braz. J. Med. Biol. Res. 41 (2008) 589.
- [2] S. Shao, J. Qiu, Acta Phys. Chim. Sinica 25 (2009) 1342.

- [3] P. Martinez-Landeira, J.M. Ruso, G. Prieto, F. Sarmiento, M.N. Jones, *Langmuir* 18 (2002) 3300.
- [4] J. Flarakos, K.L. Morand, P. Vouros, *Anal. Chem.* 77 (2005) 1345.
- [5] N. Zhou, Y.Z. Liang, P. Wang, *J. Photochem. Photobiol. A* 185 (2007) 271.
- [6] L. Shang, X. Jiang, S. Dong, *J. Photochem. Photobiol. A* 184 (2006) 93.
- [7] T.O. Hushcha, A.I. Luiik, Y.N. Naboka, *Talanta* 53 (2000) 29.
- [8] T. Peters, *All About Albumin. Biochemistry, Genetics and Medical Application*, Academic Press, San Diego, 1996.
- [9] D.C. Carter, J.X. Ho, *Adv. Protein Chem.* 45 (1994) 153.
- [10] P.K. Singh, D.N. Kumar, *Spectrochim. Acta A* 64 (2006) 853.
- [11] J.J. Sha, M.H. Zhang, Y.J. Jiang, *The Handbook of New Breed Pesticide of Overseas*, Chemical Industry Press, Beijing, 1993.
- [12] M. Katyal, Y. Dutt, *Talanta* 22 (1975) 151.
- [13] B. Singh, R. Shrivastava, K.K. Narang, *Synth. React. Inorg. Met.Org. Chem.* 30 (2000) 1175.
- [14] E. Vinuelas-Zahinos, M.A. Maldonado-Rogado, F. Luna-Giles, F.J. Barros-Garcia, *Polyhedron* 27 (2008) 879.
- [15] P. Vicini, F. Zani, P. Cozzini, I. Doytchinova, *Eur. J. Med. Chem.* 37 (2002) 553.
- [16] B.K. Kaymakcioglu, S. Rollas, *Farmaco* 57 (2002) 595.
- [17] J.V. Ragavendran, D. Sriram, S.K. Patel, I.V. Reddy, N. Bharathwajan, J. Stables, P. Yogeewari, *Eur. J. Med. Chem.* 42 (2007) 146.
- [18] H.J.C. Bezerra-Netto, D.I. Lacerda, A.L.P. Miranda, H.M. Alves, E.J. Barreiro, C.A.M. Fraga, *Bioorg. Med. Chem.* 14 (2006) 7924.
- [19] S. Rollas, S.G. Kucukguzel, *Molecules* 12 (2007) 1910.
- [20] J.D. Ranford, J.J. Vittal, Y.M. Wang, *Inorg. Chem.* 37 (1998) 1226.
- [21] J.L. Buss, B.T. Greene, J. Turner, F.M. Torti, S.V. Torti, *Curr. Top. Med. Chem.* 4 (2004) 1623.
- [22] P.S. Donnelly, A. Caragounis, T. Du, K.M. Loughton, I. Volitakis, R.A. Cherny, R.A. Sharples, A.F. Hill, Q.-X. Li, C.L. Masters, K.J. Barnham, A.R. White, *J. Biol. Chem.* 283 (2008) 4568.
- [23] G.M. Sheldrick, *Acta Cryst. A* 64 (2008) 112.
- [24] A.L. Spek, *Acta Cryst. D* 65 (2009) 148.
- [25] L.M. Venanzi, *J. Chem. Soc.* (1958) 719.
- [26] P. Krishnamoorthy, P. Sathyadevi, A.H. Cowley, R.R. Butorac, N. Dharmaraj, *Eur. J. Med. Chem.* 46 (2011) 3376.
- [27] T. Nash, *Biochem. J.* 55 (1953) 416.
- [28] L.C. Green, D.A. Wagner, J. Glogowski, P.L. Skipper, J.S. Wishnok, S.R. Tannenbaum, *Anal. Biochem.* 126 (1982) 131.
- [29] H.H. Draper, M. Hadley, *Methods Enzymol.* 186 (1990) 421.
- [30] J.G. Collee, J.P. Duguid, A.G. Farser, B.D. Marmion, *Practical Medical Microbiology*, Churchill Livingstone, New York, 1989.
- [31] S.N. Rao, K.N. Munshi, N.N. Rao, M.M. Bhadbhade, E. Suresh, *Polyhedron* 18 (1999) 2491.
- [32] H. Temel, U. Cakir, B. Otludil, H.I. Ugras, *Synth. React. Inorg. Met. Org. Chem.* 31 (2001) 1323.
- [33] M.R. Maurya, S. Khurana, C. Schulzke, D. Rehder, *Eur. J. Inorg. Chem.* (2001) 779.
- [34] T. Ghosh, S. Bhattacharya, A. Das, G. Mukherjee, M.G.B. Drew, *Inorg. Chim. Acta* 358 (2005) 989.
- [35] S.P. Perlepes, D. Nicholls, M.R. Harrison, *Inorg. Chim. Acta* 102 (1985) 137.
- [36] T. Ghosh, B. Mondal, Tarun Ghosh, M. Sutradhar, G. Mukherjee, M.G.B. Drew, *Inorg. Chim. Acta* 360 (2007) 1753.
- [37] M. Kandaz, I. Yilmaz, S. Keskin, A. Koca, *Polyhedron* 21 (2002) 825.
- [38] Y. Shen, Y. Zhang, Y. Li, X. Tao, Y. Wang, *Inorg. Chim. Acta* 360 (2007) 1628.
- [39] Lakowicz, R. Joseph, *Principles of Fluorescence Spectroscopy*, third ed., Springer, 2006.
- [40] R. Tang, Chunhua Tang, Changquan Tang, *J. Organomet. Chem.* 696 (2011) 2040.
- [41] X.Z. Feng, Z. Yang, L.J. Wang, C. Bai, *Talanta* 47 (1998) 1223.
- [42] C.X. Wang, F.F. Yan, Y.X. Zhang, L. Ye, *J. Photochem. Photobiol. A* 192 (2007) 23.
- [43] B. Liu, Y. Guo, J. Wang, R. Xu, X. Wang, D. Wang, L.Q. Zhang, Y.N. Xu, *J. Lumin.* 130 (2010) 1036.
- [44] N. Udilova, A.V. Kozlov, W. Bieberschulte, K. Frei, K. Ehrenberger, H. Nohl, *Biochem. Pharm.* 65 (2003) 59.
- [45] O.I. Aruoma, *Asia Pac. J. Clin. Nutr.* 8 (1999) 53.
- [46] M.J. Miller, H. Sadowska-Krowicka, S. Chotinaruemol, J.L. Kakkis, D.A. Clark, *J. Pharmacol. Exp. Ther.* 264 (1993) 11.
- [47] S. Moncada, A. Higgs, *N. Engl. J. Med.* 329 (1993) 2002.
- [48] A.A. Ansari, *J. Coord. Chem.* 61 (2008) 3869.
- [49] W. Levingson, P. Mikeleus, J. Jackson, W. Kaska, G.N. Schranzer, *Inorganic and Nutritional Aspects of Cancer*, Plenum Press, New York, 1978.
- [50] C.J. Ballhausen, *An Introduction to Ligand Field*, McGraw Hill, New York, 1962.
- [51] A.B.P. Lever, *Inorganic Electronic Spectroscopy*, Elsevier, Amsterdam, 1984.
- [52] B.N. Meyer, N.R. Ferrigni, J.E. Putnam, L.B. Jacobsen, D.E. Nichols, J.L. McLaughlin, *Planta Med.* 45 (1982) 31.
- [53] Z.H. Chohan, A. Scozzafava, C.T. Supuran, *J. Enzyme, Inhib. Med. Chem.* 17 (2002) 261.
- [54] Z.H. Chohan, H. Pervez, M.K. Khan, A. Rauf, C.T. Supuran, *J. Enzyme, Inhib. Med. Chem.* 19 (2004) 85.